FRACTURES, FAULTS, AND THE NONLINEAR RTM DYNAMICS OF SEDIMENTARY BASINS

K. TUNCAY*, A. PARK†, AND P. ORTOLEVA†

Abstract. A unique 3-D computer simulator is used to predict natural fracture network characteristics in the subsurface. The model is based on the numerical solution of rock deformation processes coupled to the myriad of other basin reaction, transport and mechanical (RTM) processes. The model integrates seismic, well log and surface geological data to arrive at a quantitative picture of the distribution of fractures, stress, petroleum and porosity, grain size and other textural information.

The core of the model is an incremental stress rheology that accounts for poroelasticity, nonlinear viscosity with yield/faulting, pressure solution and fracturing. In this way it couples mechanics to multi-phase flow and diagenesis (through their influenc on effective stress and rock rheological properties). The model is fully 3-D in terms of the full range of fracture orientations and the tensorial nature of stress, deformation and permeability, as well as all conservation of mass, energy and momentum solvers. The model is fully dynamic as all rock properties (rheologic, multi-phase fluid transport, grain shape, etc.) are coevolved with the other variables.

1. Introduction. Fracturing in the subsurface is key to the understanding of many fundamental and applied issues in the geosciences. The objective of this study is to show that these rock failure processes are very dynamic and that this dynamic can only be understood via a model that includes a wide range of other crustal processes. Indeed, the evolution of a fracture network is the result of the interplay of internal processes (matrix texture and pore fluid reactions and flow) and overall tectonic factors. We present results of a unique three-dimensional model of the coevolution of these dynamic phenomena for use in fundamental crustal studies and the petroleum E&P analysis. Fractures and faults affect and are affected by many processes. For example, fractures are affected by fluid pressure and, through their influence on permeability, fractures affect fluid flow and hence fluid pressure. As this is just one of many such "feedback" relations embedded in the network of geological reaction, transport and mechanical (RTM) processes, a predictive fracture model must be fully coupled (see Fig. 1). As lithologic bodies, folds, domes, salt diapirs and other features are fundamentally three dimensional (3-D), a predictive model of fracture and fault phenomena must be 3-D.

Here we present a unique 3-D RTM model capable of predicting a host of fracture and fault phenomena. Our model is based on the finite element solution of equations of rock deformation, fracture network statistical dynamics, rock failure and gouge, multi-phase flow, organic and inorganic diagenesis, pressure solution and other compaction mechanisms, and heat

*Department of Geochemistry, Faculty of Earth Sciences, Utrecht University, P.O. Box 80021, 3508 TA Utrecht, The Netherlands.

†Laboratory for Computational Geodynamics, Indiana University, Chemistry Building, Bloomington, IN 47405.

J. Chadam et al. (eds.), *Resource Recovery, Confinement, and Remediation of Environmental Hazards*

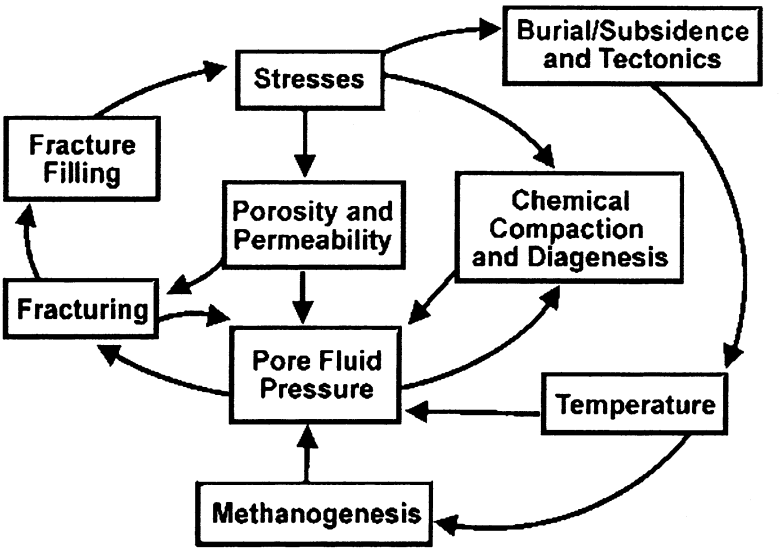

FIG. 1. *Complex network of coupled processes underlying the dynamics of a sedimentary basin. These factors and their coupling are accounted for in our unique basin simulator.*

transfer. The RTM equations are solved consistent with the influences at the boundary of the basin (sedimentation/erosion, basement heat flux, climate, sea level, and extension/compression or uplift/subsidence history) as suggested in Fig. 2.

Key to the attainment of predictive power is the coevolution of all variables. Thus, flow changes fluid pressure which can cause fractures and thereby direct fluid flow along preferred fracture directions. Such coupling and coevolution must be accounted for in their full 3-D manifestation. We compute the dynamics of the evolving probability distribution of fracture length, aperture and orientation. Properties such as the permeability tensor are functionals of this probability distribution and constitutes a key element of many crustal fluid migration phenomena.

The challenge of modeling fractures and faults in reservoir or basin scale systems is one of scale. Typically fractures are meter scale in length and sub-millimeter scale in aperture. Clearly, it is not feasible to model fractures by introducing a sub-millimeter scale numerical grid across the reservoir or basin.

The solution is to introduce variables such as average local fracture length, aperture and orientation. Characterizing the "typical" fracture in a macrovolume element of the system. By definition, a macrovolume element is smaller than the scale of the phenomenon of interest (a reservoir) but large enough to contain a statistically significant number of fractures.

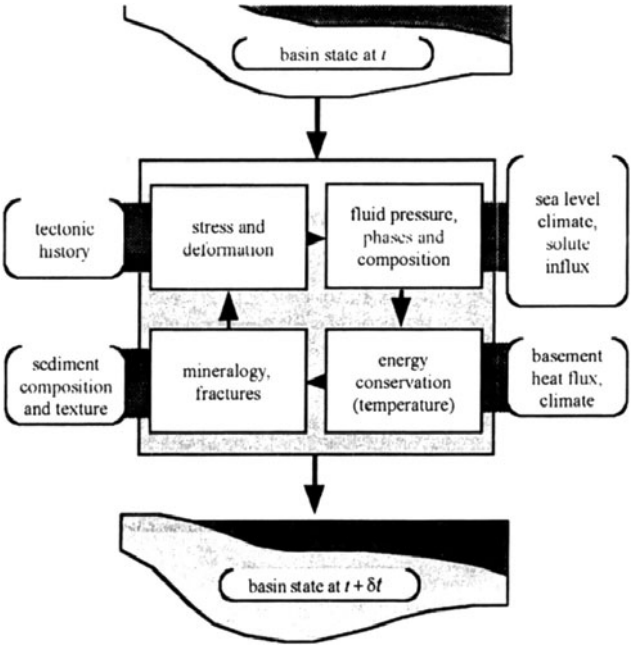

FIG. 2. *Schematic flow chart showing the interplay of geological data and the internal RTM processes in evolving a basin over one computational time step.*

Such a theory is thus, by nature, a statistical model with the macrovolume element as the sampling volume.

Within such a framework, the variables characterizing the fracture network obey ordinary differential equations in a rock-fixed reference frame (i.e., one moving with the velocity of deformation of the solids). Letting Θ be a collection of texture variables characterizing the fractures as well as the size, shape, orientation, packing, and mineralogy of the grains, we have

$$\frac{D\Theta}{Dt} = A(\Theta, \underline{\underline{\sigma}}, f, T) \tag{1.1}$$

where $\underline{\underline{\sigma}}$ is the stress on and f and T are the fluid properties (phase and composition) and temperature in the macrovolume element. In this way fractures (and in general texture dynamics) couples to stress and other factors. Furthermore, rock rheology depends on Θ (as well as f and T), completing a stress/deformation $\Leftrightarrow$ texture feedback. This is just one of the feedback loops contained in Fig. 1. Introducing the concept of texture dynamics and capturing the many coupling relations driving the dynamic crustal system is at the heart of our fracture and fault prediction approach. In the remainder of this paper, we illustrate the comprehensiveness and power of our approach using a number of examples. Applications to petroleum E&P and the fundamentally 3-D nature of many crustal RTM phenomena are noted.

2. The basin RTM simulator.

2.1. Purpose. An overview of our Basin RTM simulator used for fracture and fault modeling is as follows. A complex network of geochemical reactions, fluid and energy transport and rock mechanical (RTM) processes underlies the genesis, dynamics and present-day characteristics of petroleum reservoirs or other crustal phenomena in Basin RTM (see Fig. 1). Basin RTM integrates all the relevant geological factors and RTM processes believed to operate in a sedimentary basin. As reservoirs are fundamentally three-dimensional in nature, Basin RTM is fully 3-D.

The RTM processes and geological factors accounted for in Basin RTM are outlined in Fig. 2. External influences such as sediment input, sea level, thermal and tectonic effects are allowed to influence the progress of internal RTM processes. Within the basin, these RTM processes modify the sediment chemically and mechanically to arrive at petroleum and mineral reserves, basin compartments and other internal features.

Basin RTM provides a platform for integrating all available geological data as suggested in Fig. 2 using the framework provided by the laws of physics and chemistry to facilitate the of exploration or field development. Available information can be divided into geological data and the physico-chemical rate laws and parameters. The former make a simulation tailored to the specific basin. The physico-chemical information gives Basin RTM the power to predict resource location and characteristics and other features of the evolving basin.

Basin RTM can also be used to carry out sensitivity analyses or to identify new phenomena such as self-organization and other nonlinear effects that can dramatically affect the disposition of reservoirs in a basin (Ortoleva 1990, 1994a, Renard and Ortoleva 2001). Basin RTM simulations show that the sedimentary basin or other crustal system is highly dynamic, exhibiting a strong degree of autonomy, rather than simply responding to the details of the external influences. As Basin RTM uses data on present-day localtime and characteristics of lithologies to extrapolate these properties beyond the locations of this data, it enhances the use and interpretation of seismic, well log, surface geological and other data to understand the present-day and historical state of the crust. Basin RTM can be used to identify windows of time during which formations along a proposed migration pathway were open, and not blocked due to compaction, fracture closure or diagenetic cementation. Alternatively, Basin RTM can predict if and when a seal was breached and some of the hydrocarbons have escaped due to natural fracturing or permeability-enhancing diagenetic reactions (see Figs. 3–5).

2.2. How basin RTM works. Basin RTM makes its predictions in a completely self-consistent way through a set of multi-phase, organic and inorganic, reaction-transport modules. Calculations of all effects are done self-consistently to preserve all cross-couplings between processes

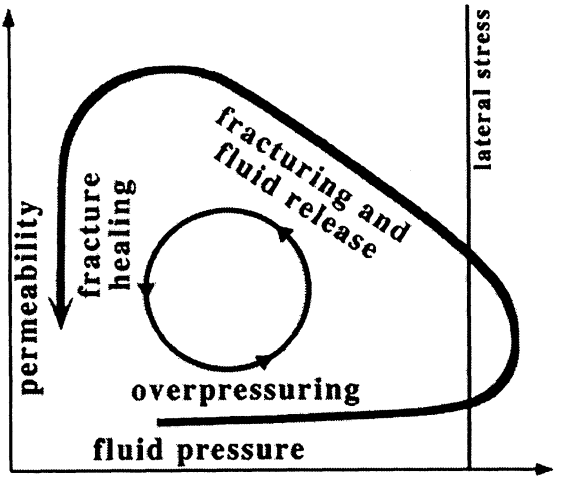

FIG. 3. *Fluid pressuring, fracturing and fracture healing feedback cycle, one example of the many feedback mechanisms inherent in the RTM process network. This cycle can repeat many times during a basin's evolution when conditions are appropriate.*

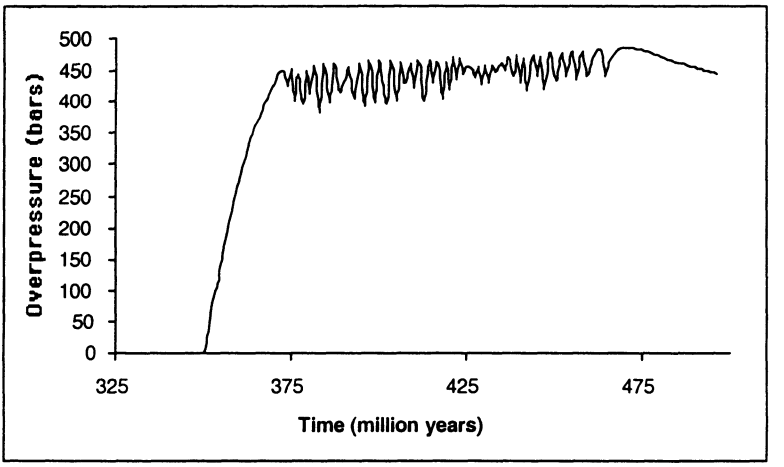

FIG. 4. *Evolution of overpressure at the bottom of the Ellenburger Formation. Overpressuring starts around 350 million years into the simulation, when fractures in the layer above the source rock disappear. Oscillatory behavior is a result of cyclic fracturing of the seal driven by petroleum generation. After 470 My the cyclic petroleum expulsion ceases and the pressure, oil saturation fracturing and other variables show a more steady behavior.*

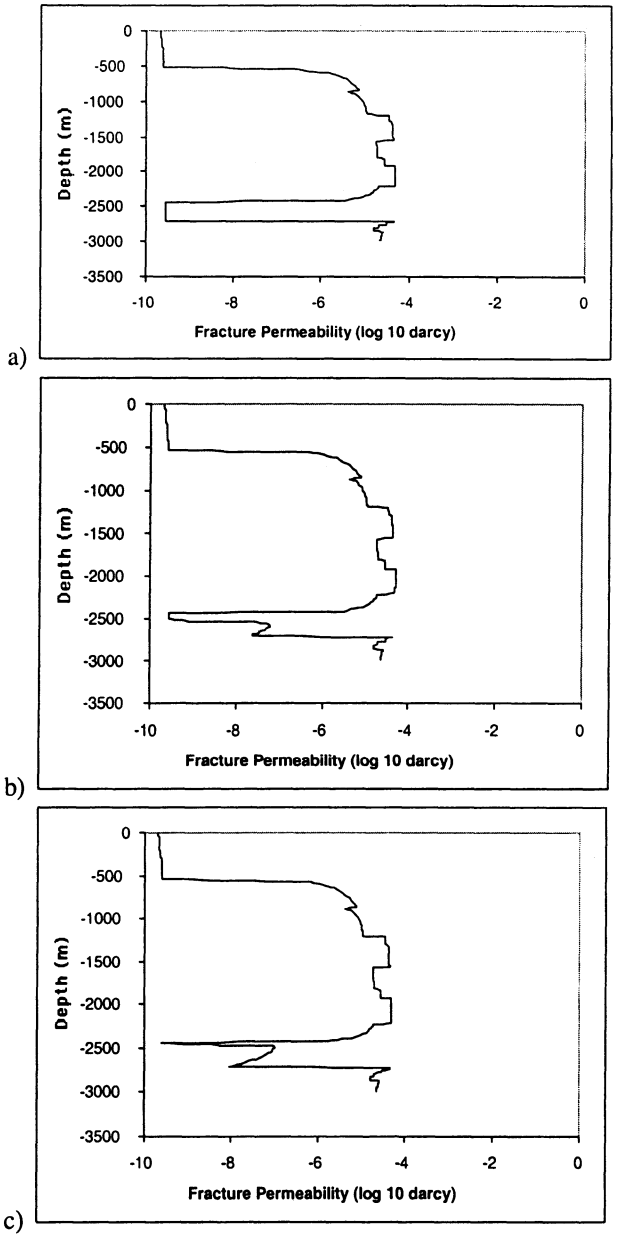

FIG. 5. *Fracture permeability profile sequence illustrating the fracture front moving through the seal (between 2450 and 2700 meters). Overpressuring of oil and water phases primarily due to oil generation creates a fracture front moving upward through the seal. Once the overpressure is released, the fractures close, which in turn results in descent of the fracture front and overpressuring restarts. This cycle continues until the oil generation rate shows down, or the seal remains fractured due to tectonic effects.*

(see Fig. 1). For example, the determination of temperature is affected by transport, which is affected by the changes of porosity that evolves due to temperature-dependent reaction rates. Similarly, the rate of kerogen decomposition depends on temperature which, in turn, depends on thermal transport that is affected, through fluid buoyancy, thermal conductivity, capillarity and relative permeability, by the content of organic material and its thermal decay. All such coupling relations between the full set of RTM processes as in Fig. 1 are accounted for in our model.

Predictive power is limited for less rigorous approaches that use statistical correlations. For example, in such methods, porosity history is often based on a formula relating it to mineralogy and depth of burial. However, porosity evolves due to the detailed stress, fluid composition and pressure, and thermal histories. These histories are different for every basin. Thus a simple correlation of porosity with depth and lithologic type does not exist in principle. Basin RTM avoids such problems by solving the fully coupled rock deformation, fluid and mineral reaction, fluid transport and heat transfer problems. Finally, statistical correlations give the average behavior. As "on the average" there are no interesting features such as producible pools of petroleum, such approaches can only have a limited interest.

The interplay of geological and physico-chemical information in Basin RTM is suggested in Fig. 2. Consider one forward time step in a Basin RTM simulation. The purpose of the incremental evolution step is to advance the state of the basin from a time t to a later time $t + \delta t$. Two distinct operations take place simultaneously during this time interval δt. The geological information is used to 1) fix the input/output of energy and mass at the basin boundaries and 2) impose the tectonic history (i.e., the overall basin deformation or stress) at the basin boundaries. On the other hand, the physico-chemical processes are used to determine the evolution in δt of the spatial distribution of the local state. The latter describes stress, fluid properties, mineral content, rock texture, permeability, fracture characteristics and temperature.

Basin RTM geological input data is divided into four categories as shown in Fig. 2. The tectonic data gives the change in the lateral extent and the shape of the basement-sediment interface during δt. As suggested in Figs. 2, this data provides the conditions at the basin boundaries needed to calculate the change in the spatial distribution of stress and rock deformation within the basin. This latter physico-chemical calculation is carried out by a stress module that solves equations for incremental stress rock rheology and force balance (see Subsection 3.3 below).

The next type of Basin RTM geological data is that affecting the fluid transport, pressure and composition. This fluid data includes sea level changes, basin recharge conditions and the composition of fluids injected from the ocean, meteoric and basement sources. This history of boundary input data is then used by the hydrologic and chemical modules to calculate

the evolution of the spatial distribution of fluid pressure, fluid composition and fluid phases within the basin. These physico-chemical calculations are based on single or multi-phase flow in a porous medium and on fluid phase molecular species conservation of mass (i.e., the reaction-transport equations). The physico-chemical equations draw on internal data banks for permeability-rock texture relations, relative permeability formulae, chemical reaction rate laws and reaction and phase-equilibrium thermodynamics.

The spatial distribution of heat flux imposed at the bottom of the basin is another geological input/control. This data as well as the temperature imposed at the top of the sediment pile (i.e., climate and ocean-bottom temperature) is used to evolve the spatial distribution of temperature within the basin during the time interval δt. This evolution is computed using the equations of energy conservation and data for mineral and rock thermal properties (conductivities and specific heats).

The sedimentation data provides the detailed textural characteristics such as grain size, shape, mineralogy, mode and organic texture of the sediment being deposited during δt. This history is automatically computed by Basin RTM using interpreted well log, seismic core and surface data. The physico-chemical laws and data are used to calculate the change of the spatial distribution of mineral and organic texture within the basin during δt. These physico-chemical calculations involve the rate laws for free face grain chemical kinetics, pressure solution and grain rotation or breakage, grain nucleation and the laws of kerogen chemical kinetic transformation. Also used are the laws of fracture nucleation, extension, aperture dynamics and the kinetics of cement infilling.

All this geological input data and physico-chemical calculations are integrated in Basin RTM over many time steps δt to arrive at a prediction of the evolution history and the present-day internal state of a basin or field. In this way, the physico-chemical laws are used to translate the geological input data into a prediction of the changes of internal basin state and its evolution over a basin's history from its inception (or other chosen initial state) to the present.

2.3. Applications of basin RTM to sedimentary basins. Other basin models have been used to gain valuable insights into the petroleum system. Typically these models are 2-D and treat only two or three processes (Maubeuge and Lerche 1993, 1994; Roberts and Nunn 1995; Wang and Xie 1998; Ungerer et al. 1990; Schneider et al. 1996; Luo and Vasseur 1996; Larson et al. 1993; Luo et al. 1998). Consequently, they are not sufficiently comprehensive to accurately simulate natural sedimentary systems and, in particular, fracture networks.

Fracture-mediated petroleum expulsion, migration, and escape from reservoirs are key aspects of the dynamic petroleum system (Figs. 3–5). In most of the existing basin evolution models, it is assumed that rocks fracture when the fluid pressure exceeds a specified fraction of lithostatic

stress (Maubeuge and Lerche 1993, 1994; Roberts and Nunn 1995; Wang and Xie 1998). This assumption ignores the dependence of fracturing on lithologic properties. In our studies, we find that fracturing strongly depends on rock composition and texture, including mineralogy, grain size, and porosity which indirectly affect the stress tensor (Figs. 6, 7). Another limiting assumption is that there exists a simple dependence of porosity on effective stress (Maubeuge and Lerche 1993, 1994; Roberts and Nunn 1995; Wang and Xie 1998; Ungerer et al. 1990; Schneider et al. 1996; Luo and Vasseur 1996). This results in a very smooth porosity profile but ignores the dependence of porosity on rock composition and texture. In our approach, porosity is obtained by both solving the mass balance equation for solids and computing rock deformation velocity using a multi-process, incremental stress rheology that contains the elastic and viscous parameters which are functions of texture and composition. By coupling mass balance algorithms with our porosity and stress solvers, porosity and stress are computed self-consistently. As a result, shales usually have lower porosity, and higher least compressive stress than sandstones (Fig. 7). The small grain size combined with low porosity results in very low permeability and thus these layers can form efficient seals. Furthermore, our results show that low shear viscosity/bulk viscosity ratio makes fracturing very unlikely in the absence of flexure or extreme overpressuring mechanisms like petroleum generation or fluid thermal expansion.

In other basin evolution simulators, fracture permeability is assumed to be isotropic. This simplification ignores the fact that, for an accurate description of fracture orientations, the full stress tensor as well as irreversible (e.g., viscous-like rather than purely elastic) behavior must be known. Also disregarded is the interaction between the deformation/stress computation and fracturing. Rocks fracture due to the difference between fluid pressure and least compressive stress. But as fractures open, overall rock volume increases and fluid pressure in the fractures compresses the rock, increasing the compressive stress normal to the fracture plane. Thus, fracturing is a self-limiting process; firstly, as fractures open, they provide a pathway for fluid escape, and secondly, the volumetric strain caused by fractures increases the confining stress that reduces the rate of fracture growth (Tuncay, Park and Ortoleva 2000a,b).

Although one- and two-dimensional studies give hints about the dynamics of basin evolution, a three-dimensional basin simulator is necessary to take three-dimensional geometric effects into account. This becomes extremely important when fracturing is due mainly to flexure and the direction of tectonic compression/extension is changing during the basin's history. Fracture networks provide a pathway for fluid flow and, especially in layered rocks, fluids can move laterally out of the vertical plane. Appropriate simulations can be accomplished only by a three-dimensional basin simulator with a stress/deformation solver that can capture nonplanar effects and strong contrasts in rheology from layer to layer.

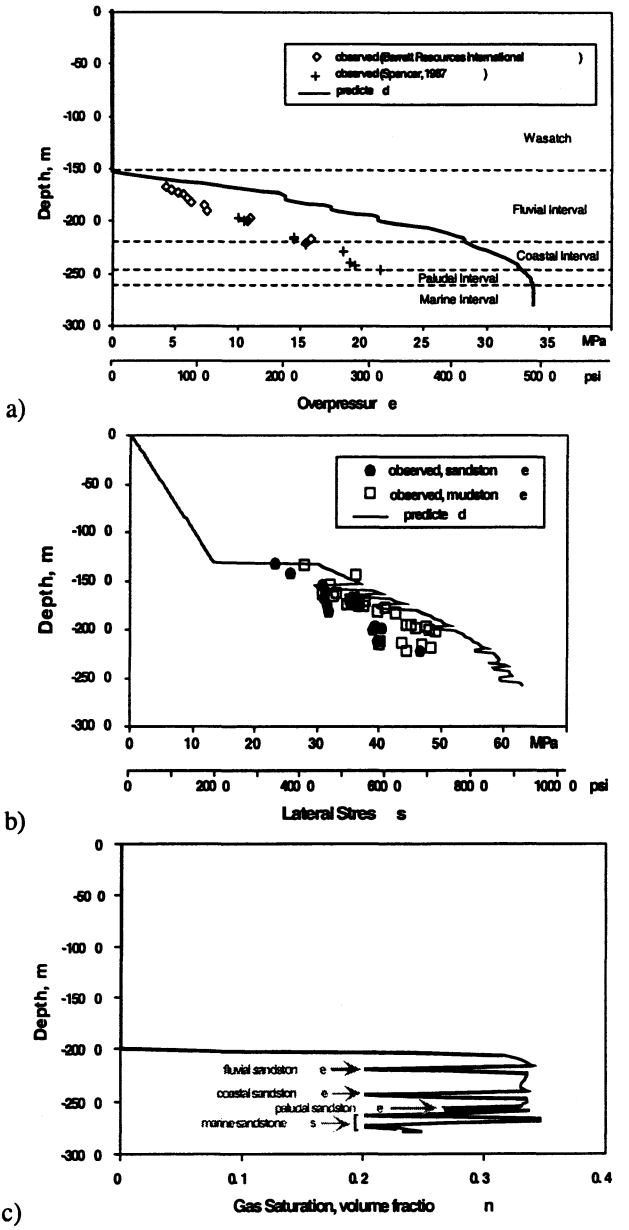

FIG. 6. *Simulations by Basin RTM show good agreement with observations. Shown are present-day fluid pressure (a) and least compressive stress at the MWX site, Piceance Basin, Colorado compared with observations. In sandstones, the lateral stress and fluid pressures are found to be similar, indicating their vulnerability to fracturing whereas in the mudstones lateral stress exceeds fluid pressure, underscoring the lack of fracturing in them at present day (as observed). Our predictions also show that this situation is dynamic—during an epoch in the past, some of the mudstones were also fractured in some areas in the Piceance Basin as suggested in the literature. (c) Predicted natural gas saturation (from Payne et al. 2000).*

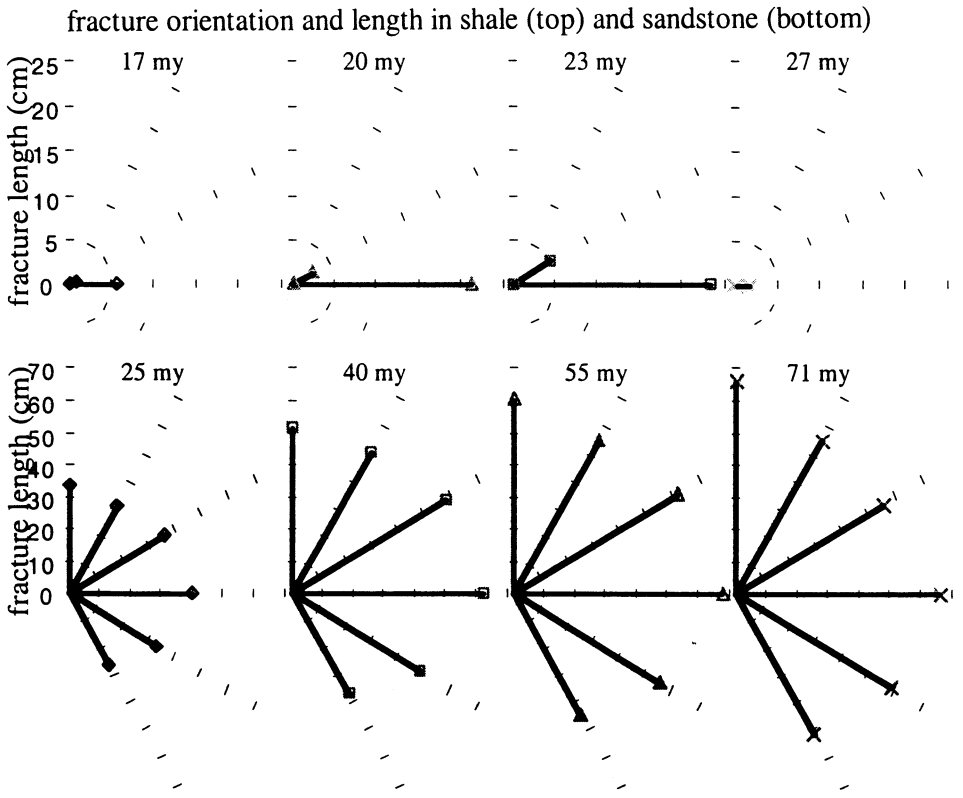

FIG. 7. *Predicted fracture orientations and length in a shale (top) and a sandstone (bottom) from a Piceance Basin simulation. Changing sediment properties, stress and fluid pressure during the evolution of the basin result in dynamic fracture patterns, which in turn significantly affect the anisotropy of fracture permeability. If the enhanced permeability from fracturing is significant, it can direct the flow of petroleum; understanding such occurrences of the past, therefore, can be important for identifying or understanding reservoirs in presently unlikely structural and stratigraphic locations.*

Although the history of temperature, sedimentation rate, and subsidence rate are among the most important parameters that affect the evolution of a basin, some basin simulators start with a predefined grid (Schneider et al. 1996). In other words, two basins with the same final thickness and lithology but different time history are assumed to behave similarly. This approach ignores the time-dependence of, for example, overpressuring which often correlates with sedimentation rate and is a key factor in fracturing as well as deformation (Wang and Xie 1998; Ortoleva 1998).

Our model accounts for the changing rock rheological parameters that accompany the changing lithologic and fracture properties. The bulk, shear and effective stress coefficients of the (assumed) isotropic rocks are computed using Berryman's composite medium theory (Berryman 1980, 1986). In our approach, by assuming that the shear and bulk viscosities depend on

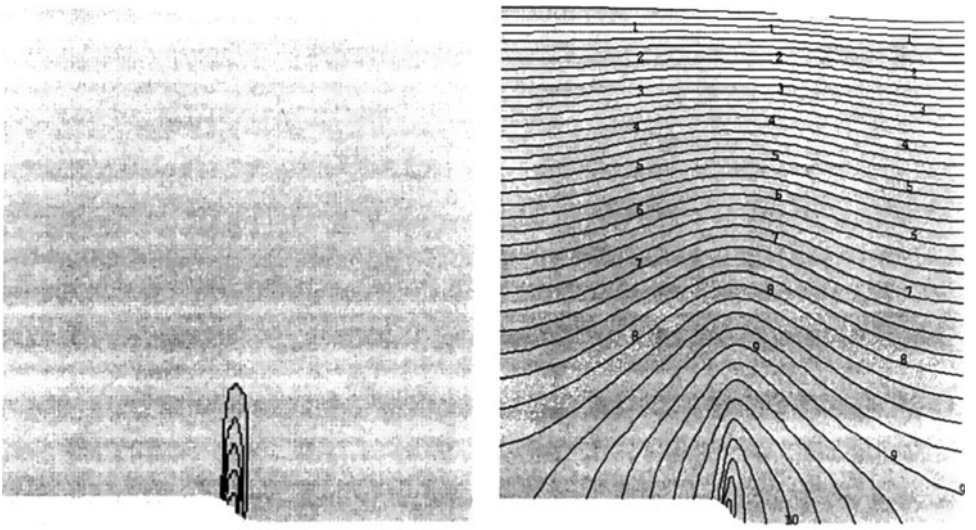

FIG. 8. *The effect of gouge on a) porosity and b) overpressure. The size of the domain is 3 km by 3 km in cross-section. The fault width is 0.1 km and the rate of faulting is 0.2 km/million years. To isolate the effect of gouge on the pressure and texture, a very high bulk viscosity is used. Therefore, the only overpressuring mechanism present is the gouge-related changes in the texture.*

grain contact areas, rheology is computed as a function of the mechanically and diagenetically modified texture. Thus, dynamic rheologic properties are used to compute basin stress/deformation history using an incremental stress rheology (Zienkiewicz and Cormeau 1974; Rice 1975) extended by the authors(Tuncay, Park and Ortoleva 2000a,b; Ortoleva 1994a, 1998).

Another limitation of previous models is the absence of shear failure. Only a few models consider the contribution of mechanical shear to rock failure (Luo et al. 1998; Larson et al. 1993). However, these models are limited to two dimensions. In our model, a Drucker-Prager-type failure function is used to build in a shear failure via a transition in rock viscosity. As the rock approaches failure, shear viscosity decreases. This feature extends the applicability of our basin simulator to fault formation problems (Figs. 8 and 9). We have already made an attempt to include the rate of strain due to gouge (Fig. 8) to show the effect of shearing on the particle size distribution and porosity (Ozkan and Ortoleva 2000). A preliminary normal faulting simulation is seen in Fig. 9 where an intact rock is sheared, a fault develops. The computational domain (initially consisted of intact granite) is 6 km by 9 km in cross section. The velocity of vertical movement on the right side is 1 km/million years. The temporal complexity of fluid pressure in a faulting system is shown in Fig. 10. The overpressure

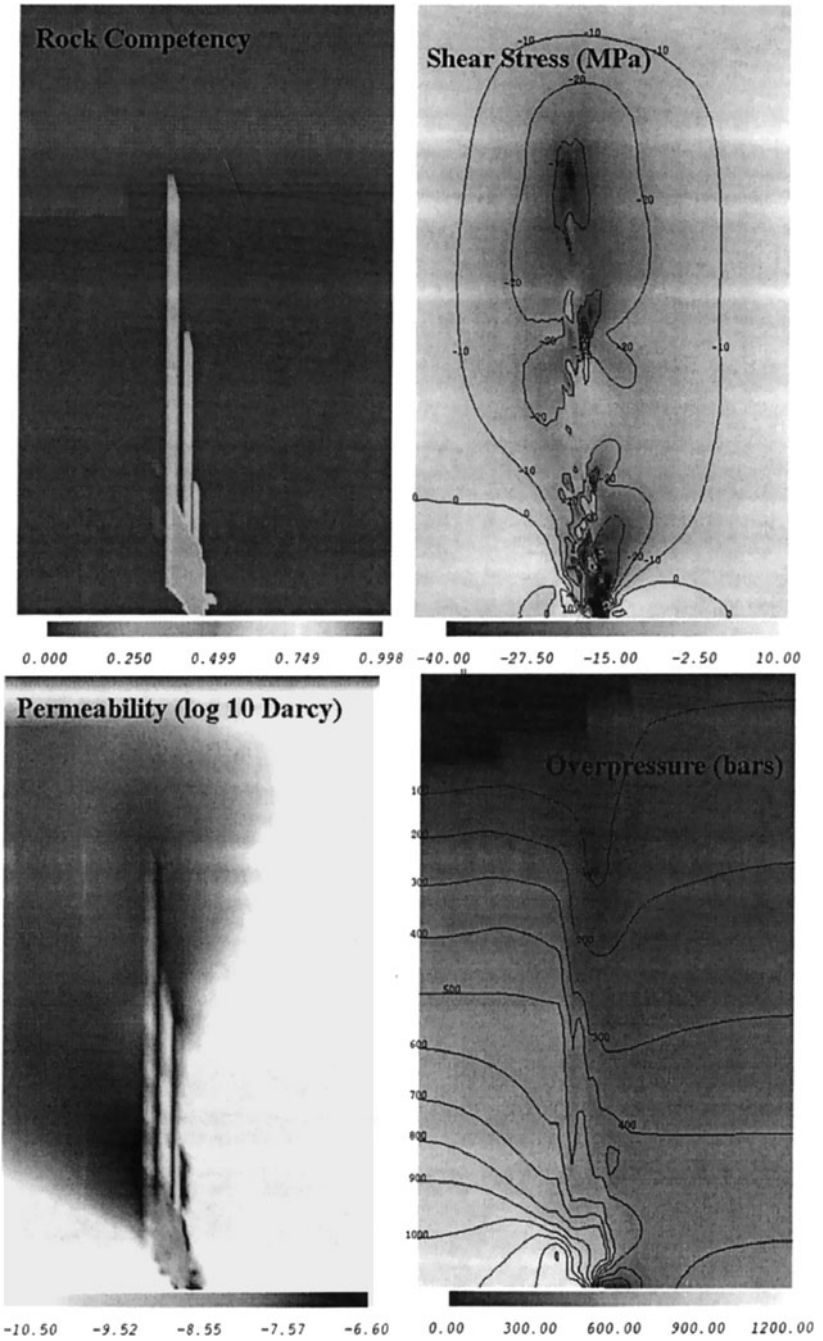

FIG. 9. *Simulation of normal faulting. The computational domain (initially consisted of homogeneous intact granite) is 6 km by 9 km in cross section. The velocity of vertical movement on the right side is 1 km / million years. Note the stress concentration that develops at the fault tips in association with upward growth. Broken grain-grain contacts increase permeability and significantly alter fluid pressure and fluid flow which in turn affects the rock behavior through the effective stress principle. The branching and stress heterogenity are self-organized, arising through the coupling of RTM processes accounted for in Basin RTM.*

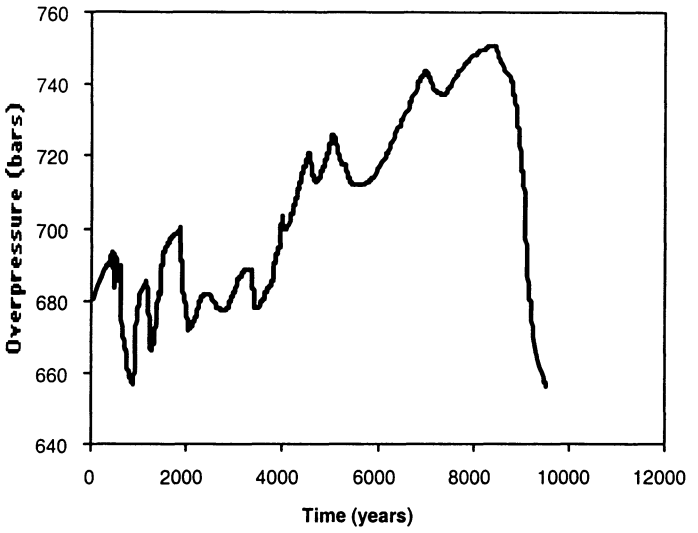

FIG. 10. *The temporal variation of overpressure at a material point located 100 m above the bottom boundary for the simulation of Fig. 9. This chaotic dynamic self-organizes even though the energy input rate to the system is constant.*

distribution as seen in Fig. 9 suggests that fluid flow pattern is dictated by faulting.

2.4. Salt tectonics. Salt movement in the subsurface can dramatically affect the distribution and character of fracture zones and faults for several reasons:

- salt diapirism and related phenomena can cause flexure and otherwise dramatically affect the stress regime in the neighboring sediments;
- salt movement can affect the topography of the sea floor and thereby the geometry and lithologic character of the salt-adjusted sediments;
- salt is of vanishingly small permeability and therefore can isolate high overpressure (up to lithostatic) and thereby influence effective stress in the underlying sediments; and
- by distorting the heat flux, changing the salinity, and altering the fluid flow patterns, salt can change the diagenetic history and, thereby, rock mechanical properties.

As salt withdrawal is believed to be an important factor in fracturing in some areas, we have incorporated advanced salt tectonics modeling into Basin RTM. With this, our simulator can address the following E&P challenges:

- predict the location and geometry of faults or zones of fracturing created by salt motion;

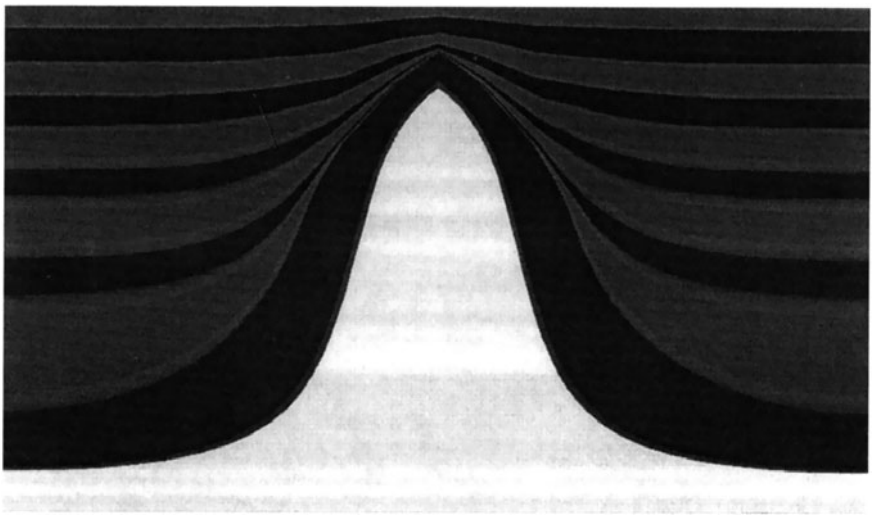

FIG. 11. *Basin RTM simulated salt wave showing associated deformation (as indicated by the shape of the evolved salt body). Shown is the state after 8 million years of deformation and sedimentation. The salt bed originally only had a 400 meter topographic contrast. There are alternating layers of sandstones and shales above the salt at this stage. The salt tectonic⇔sedimentation interaction induced the sediment geometry and the generation of mini-basins at the flanks of the wave.*

- predict the morphology of sedimentary bodies created by salt deformation;
- locate pools of petroleum or migration pathways created by salt tectonics; and
- assist in the interpretation of seismic data in salt tectonic regimes.

The interplay of salt deformation with the rheology of the surrounding strata is key to understanding the salt deformation⇔reservoir location and characteristics relationship. The continuous and discontinuous (i.e., fauting and fracturing) responses of the surrounding sediments are induced by salt movement. In turn, the deformation of these sediments promotes or inhibits salt motion (Tuncay and Ortoleva 2001).

Fig. 11 shows a cross-section of a Basin RTM-simulated salt wave. Note the relationship among deformation, fluid flow and fracturing. The latter's orientation follows salt morphology. Fluid flow patterns are strongly influenced by salt morphology and associated fracture patterns. In this case and those to follow the salt deformation is due to the interplay of salt buoyancy, slat modification of the distribution of the rate of sedimentation and the overall tectonics (i.e., basin extension/compression and upheaval/subsidence).

To predict salt tectonics-related petroleum pools, one must co-evolve petroleum generation/expulsion/migration with salt and rock deformation.

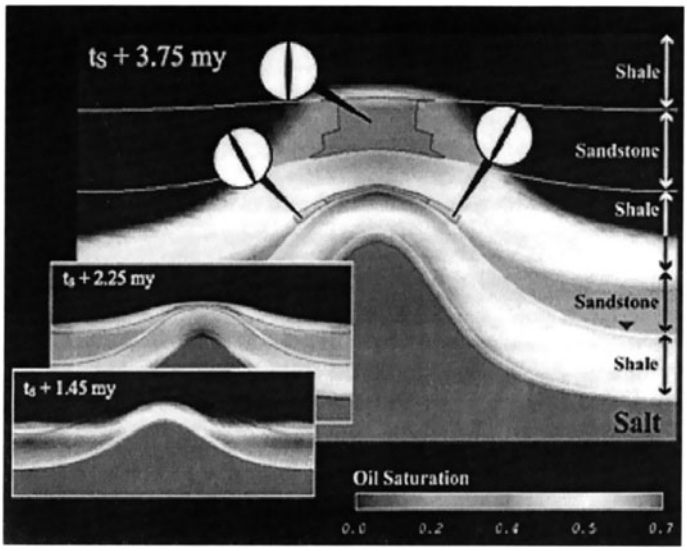

FIG. 12. *Simulated time sequence of oil saturation overlying a rising salt dome. Source rock overlying the dome was transiently overpressured and fractured, facilitating upward oil migration within it and into the overlying layers. Orientations of long-lived fractures (residing in the sandstones) illustrate the relationship between the salt motion and fracture pattern. The location of oil strongly depends on the rate of salt motion and the coevolving mechanical and transport properties of the adjacent sediments.*

Fig. 12 shows an oil pool developed in association with salt diapirism. The oil was generated in a source rock overlying the salt, both of which were essentially flat in an early stage that preceded diapirism. A similar situation but for a subsalt source rock is seen in Fig. 13. In both cases, the influence of salt motion on fracturing and porosity strongly affect migration and ultimate reservoir quality. The escape of subsalt oil at the edges of the salt lens is also seen in Fig. 13.

Salt tectonics is, for the most part, a fundamentally 3-D phenomenon. An example of a simulated salt diapir in 3-D view is seen in Fig. 14. Note the pockets of fracturing associated with the salt diapir.

3. Incremental stress rheology, statistical fracture dynamics and rock competency.

3.1. Incremental stress rheology. The strong coupling of deformation with the diagenetic, hydrologic and thermal processes is captured in Basin RTM using an incremental stress rheology. The specific rheology used in Basin RTM integrates all the strain mechanisms believed to operate in a basin. It has the form (Tuncay, Park, and Ortoleva 2000a; Ortoleva 1994a, 1998)

$$\dot{\underline{\underline{\varepsilon}}} = \dot{\underline{\underline{\varepsilon}}}^{el} + \dot{\underline{\underline{\varepsilon}}}^{vp} + \dot{\underline{\underline{\varepsilon}}}^{ps} + \dot{\underline{\underline{\varepsilon}}}^{fr} + \dot{\underline{\underline{\varepsilon}}}^{go}. \tag{3.1}$$

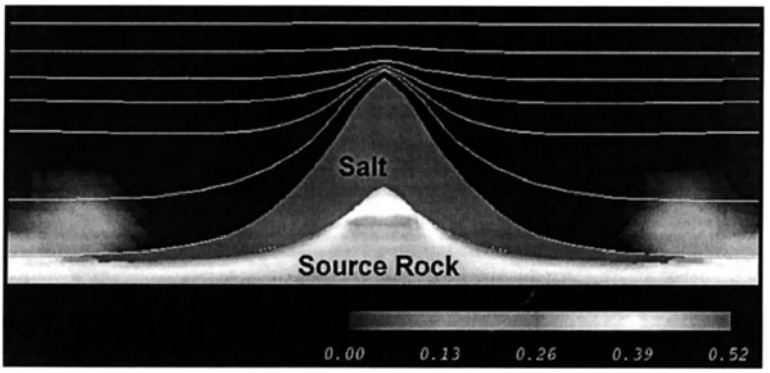

FIG. 13. *As in the previous figure except for an initially finite size (lenticular) salt body and in addition the co-evolution of subsalt petroleum. Shown is the oil saturation with curves indicating lithologic contacts. The overpressure under the salt body and the stress regime on the underlying sediment have preserved porosity in the center region under the salt while the compaction under the edge of the salt led to the formation of a seal. Thereby a subsalt compartment is formed.*

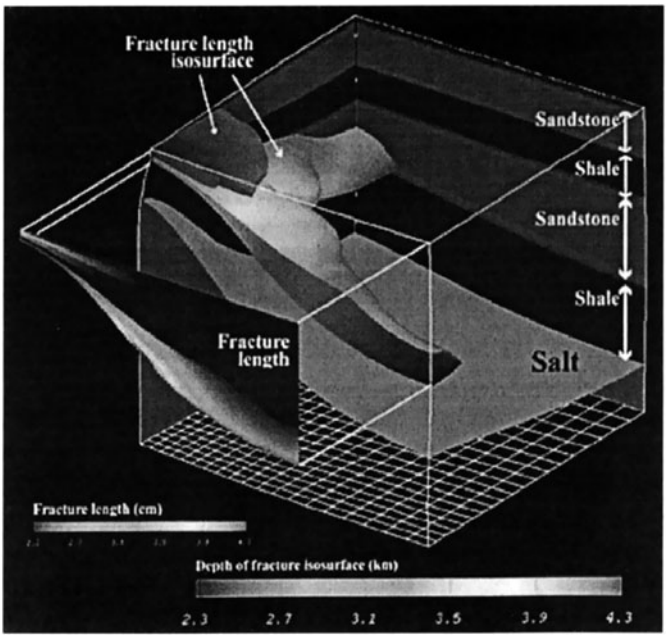

FIG. 14. *Simulated quarter section of a salt diapir showing the relationship to fracturing in the overlying sandstones after 3 million years of deformation. Extracted partial front cross section shows the fracture length.*

Here, $\dot{\underline{\underline{\varepsilon}}}$ is the net rate of strain while the terms on the right give the specifics of four processes: poroelasticity (el), continuous viscoplastic (vp), pressure solution (ps), fracturing (fr) and gouge (go). Specific expressions for each term have been taken from the literature or newly developed for our RTM simulator (see §3.1 for the development of the rate of strain tensor due to fracturing).

Let us make some of the coupling more explicit. The poroelasticity rate of strain $\dot{\underline{\underline{\varepsilon}}}^{el}$ may be expressed in terms of stress $\underline{\underline{\sigma}}$, pressure p of the wetting fluid phase, and rock texture Θ via

$$\dot{\underline{\underline{\varepsilon}}}^{el} = \underline{\underline{\underline{\underline{C}}}}^{-1}(\Theta)\frac{D}{Dt}\left(\underline{\underline{\sigma}} + \alpha(\Theta)p\underline{\underline{I}}\right) \tag{3.2}$$

for fourth rank matrix of poroelastic coefficients $\underline{\underline{\underline{\underline{C}}}}$ and effective stress coefficient α; D/Dt represents a material time derivative measuring the rate of change of a tensor in time with respect to a local reference frame fixed to a translating, rotating material volume element. The texture Θ represents a set of variables characterizing the mineralogy, shape, size, orientation and packing of the grains. In summary

$$\dot{\underline{\underline{\varepsilon}}}^{el} = \dot{\underline{\underline{\varepsilon}}}^{el}\left(\Theta, p, \underline{\underline{\sigma}}\right), \tag{3.3}$$

illustrating the strong coupling between deformation, fluid properties and texture.

A direct coupling of mechanics and chemistry arises through pressure solution. Grain dissolution at stressed grain-grain contacts induces compaction and, thereby, contributes to $\dot{\underline{\underline{\varepsilon}}}$. The rate of this pressure solution contribution, $\dot{\underline{\underline{\varepsilon}}}^{(ps)}$, depends on the stress at grain-grain contacts and, hence, on the macro-stress $\underline{\underline{\sigma}}$, fluid pressure and texture. However, $\dot{\underline{\underline{\varepsilon}}}^{(ps)}$ should also depend on the composition of the (assumed single-phase) pore fluid. The latter may be characterized by the set of concentrations $c = \{c_1, c_2, \cdots c_N\}$ for the N pore fluid species system; hence, $\dot{\underline{\underline{\varepsilon}}}^{(ps)}$ depends on $\underline{\underline{\sigma}}, \Theta, p$ and c.

As the present theory is macroscopic, the variables describing fractures are considered to be part of the texture Θ. This assumes that the length scale on which the phenomena of interest vary is much greater than the fracture length or inter-fracture spacing. Otherwise one must treat fractures individually, an approach that is not viable for basin-scale modeling. With our macro-textural description, one must allow for the potential influence of the fracture variables on rock mechanical and other properties.

One expects that $\dot{\underline{\underline{\varepsilon}}}^{(j)}$, j=poroelasticity, viscosity, pressure solution, fracturing, gouge, etc., should, in general, depend on all the aforementioned variables $\left(\underline{\underline{\sigma}}, \Theta, p, c\right)$, as well as absolute temperature T. With this,

$$\dot{\underline{\underline{\varepsilon}}} = \sum_{j=1}^{N_d} \dot{\underline{\underline{\varepsilon}}}^{(j)}(\Theta, \underline{\underline{\sigma}}, p, c, T). \tag{3.4}$$

The dependency of the $\underline{\underline{\dot{\varepsilon}}}^{(j)}$ on the indicated state variables may be nonlocal in time. For example, in the case of poroelasticity, $\underline{\underline{\dot{\varepsilon}}}^{(pe)}$ depends on the time-derivative of effective stress. Therefore, the $\underline{\underline{\dot{\varepsilon}}}^{(j)}$ may be functionals of their arguments that can, in principle, sample the state variables in some finite volume of space-time. The dependence of the strain rates on state clarifies the central role of incremental stress theory in integrating all the RTM basin processes into a unified model. It is the coupling allowed by this integration that underlies many key basin phenomena from fault dynamics to episodic fluid flow, seal formation and overpressure.

To complete the incremental stress formulation, explicit expressions for the rate functions $\underline{\underline{\dot{\varepsilon}}}^{(j)}\left(\Theta, \underline{\underline{\sigma}}, p, c, T\right)$ are required. For $\underline{\underline{\dot{\varepsilon}}}^{(ps)}$, for example, these can be obtained through geometric considerations of the texture variables and the rate of grain shortening from pressure solution (see Dewers and Ortoleva 1994a, and Ortoleva 1994a, 1998).

The total rate of strain $\underline{\underline{\dot{\varepsilon}}}$ is defined via

$$\dot{\varepsilon}_{ii'} = \frac{1}{2}\left(\frac{\partial u_i}{\partial x_{i'}} + \frac{\partial u_{i'}}{\partial x_i}\right). \tag{3.5}$$

The six independent components of the symmetric second rank tensor equation (A.3) must be supplemented with three additional equations so that the three deformation velocity components ($\underline{u} = u_1, u_2, u_3$) can be determined. The required condition arises from force balance:

$$\sum_{i'=1}^{3} \frac{\partial \sigma_{ii'}}{\partial x_{i'}} + f_i = 0 \tag{3.6}$$

for body force f_i which, for gravity, is given by

$$f_i = g\rho_m \delta_{i3}. \tag{3.7}$$

Here g is the gravitational acceleration, ρ_m is the mass density, and the 3-direction is upward.

The above formulation must be augmented with equations of texture dynamics and fluid mass and energy conservation (the latter to fix T). With this, our model provides a complete theory of basin dynamics when the equations are solved subject to the boundary conditions imposed by the overall tectonics and by the surfacial fluids (i.e., ocean bottom and atmospheric pressure).

Effects such as strain hardening or weakening are accounted for in the present model via the coupled dynamics of texture and stress. The differential equations of texture evolution introduce the time delays (memory) that make our rheology capture hardening or softening. The latter properties are reflections of texture, i.e., hardness/weakness is a unique function of texture but not of stress. Thus, rock rheology depends on texture which,

via the evolution equations of the latter, depends on the history of deformation.

In addition to the coupling of deformation to other phenomena through the incremental stress formulation, there are numerous indirect couplings. For example, rock properties such as permeability, multi-phase flow parameters, reactive grain surface area and thermal conductivity depend strongly on texture. As the latter is affected by stress and deformation, a complex network of coupling relations is thereby expressed. For further discussion of the consequence of this network, see Ortoleva (1994a,b; 1998), Tuncay, Park and Ortoleva (2000a,b), Ozkan, Tuncay and Ortoleva (1998) and Dewers and Ortoleva (1994b).

3.2. Rock competency. Sedimentary rock deformation is a multiple time and length scale phenomenon. Rocks fail rapidly but heal slowly on geological time scales (Fredrich and Evans 1992; Logan and Teufel 1986). Brittle rocks have two sources of memory. They store elastic energy, and, once failed, have broken grain-grain contacts and gouge that persist over long times. Viscous deformation or failure erase the former while chemical healing processes diminish or erase the latter. When sheared across a large-scale zone, they can fail within a meter-scale fault zone. Furthermore, the fault dynamic typically takes the form of a series of short time scale events with long inter-event healing periods to form the earthquake cycle. The challenge is to develop a rheologic model of this deformation behavior that captures this multiple scale character autonomously– i.e., from an initially uniform, unfailed system to a faulted one experiencing intermittent failure-healing cyclicity and complex spatial structure.

The rate and state dependent friction models introduce a number of state variables that are governed by ordinary differential equations (Dieterich 1979; Ruina 1983; Rice and Gu 1983; Tse and Rice 1986; Rice and Ruina 1983). The physical interpretations of these state variables are often ambiguous. A more general approach is the use of texture variables such as grain size distribution, porosity and packing as the state variables of the system. The key to this approach is that the memory of rocks is to be captured by a sufficiently rich textural model and that the texture must be coevolved with rock stress and deformation to yield a self-consistent model of strain hardening/weakening, fault narrowing and earthquake cyclicity. In the present study, these multiple scale and autonomous fault behaviors are shown to follow naturally from the feedback between stress and rock texture. Rock deformation is thereby autonomous–stress changes texture, texture changes rock rheology and, in turn, rock rheology affects stress. This feedback is shown here to be more self-consistent and fundamental than concepts such as strain hardening/weakening or velocity-dependent viscosity.

We suggest that rigorous models of rock behavior should be of the Markov type–i.e., the rate of change of rock state should only depend on

the instantaneous rock state and not on prior history. Stress and strain are related through rock rheology, to rock texture Θ (grain size, shape, packing and mineralogy). Pressure solution and grain breakage imply that the rate of change of Θ depends on stress, denoted σ. If Θ satisfies the differential equation (1.1) then in principle$\Theta(t)$ is a functional of σ, i.e. depends on $\sigma(t')$ for all $t' < t$, i.e. on the stress history: $\Theta = \Theta[\sigma]$. As rheology depends on Θ, we see that $\Theta[\sigma]$ reflects the entire prior stress history and not just the instantaneous value of σ. Clearly, however, this "memory" in a theory wherein Θ is not coevolved with σ is an artifact of the incompleteness of a rock deformation model that attempts to avoid coevolving Θ with stress. While there are many stress-strain histories that could lead to the instantaneous state of a rock, only the latter is key to predicting its failure and other behavior.

Let Γ, rock competency, measure the fraction of grain surface that is attached to other grains . Thus Γ is in the range $0 \leq \Gamma \leq 1$. Large Γ implies competency while in a low Γ rock there are few intact grain-grain contacts. Thus rheologic quantities such as rock strength or viscosity are strongly dependent on Γ.

Schematically, our model is as follows. The equation of motion of Γ is taken in the form

$$\frac{D\Gamma}{Dt} = R(\Gamma, F) \tag{3.8}$$

where F is a failure function that depends on macroscopic stress, fluid pressure, rock texture, mineralogy and temperature In three dimensions, the failure function is assumed to take the form (Drucker and Prager 1952)

$$F = aJ_1 + \sqrt{J_2} - b \tag{3.9}$$

where J_1 is the first invariant of the effective stress tensor and J_2 is the second invariant of the deviatoric effective stress tensor. The coefficients a and b can be expressed in terms of angle of internal friction φ and cohesion C determined from conventional triaxial compression experiments (Desai and Siriwardane 1984)

$$a = \frac{2\sin\varphi}{\sqrt{3}(3 - \sin\varphi)} \tag{3.10}$$

$$b = \frac{6C\cos\varphi}{\sqrt{3}(3 - \sin\varphi)}. \tag{3.11}$$

Here, we assume that cohesion depends on rock competency. For an intact rock ($\Gamma = 1$), b is large. As the rock competency is lost, the cohesion-like term b vanishes. Therefore b is a strong function of Γ taken here to be $b = b^*\Gamma^n$ where b^* refers to the value when $\Gamma = 1$ and n is a phenomenological exponent.

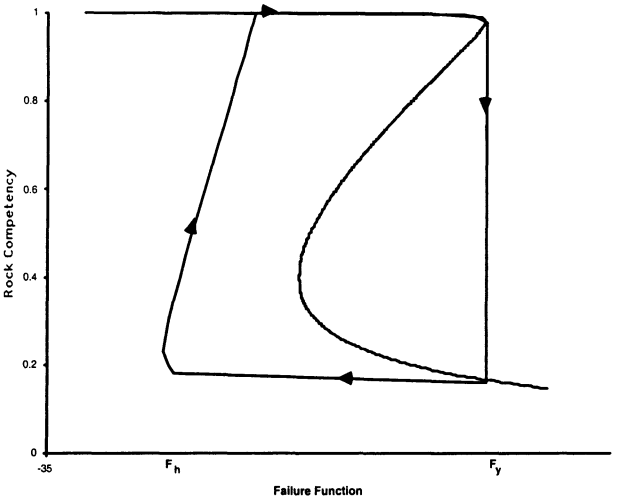

FIG. 15. *Schematic competence (Γ) and failure function (F) plane illustrating the cooperative aspects of rock failure. When Γ is near unity, the rock is competent but when F exceeds F_{yield}, it is compromised. However, for $F < F_h$, competence is regained through chemical healing processes.*

If the dynamics of Γ is relatively fast, its evolution is closely related to the shape of the curve $R(\Gamma, F) = 0$ (see Chapters 2 and 3 of Ortoleva 1992 for further discussion). The Γ-dynamics is, in a sense, a cooperative phenomenon, i.e., a decrease in competence fosters more rapid Γ decline. This is captured by the qualitative picture of Fig. 15. A schematic evolution path in the F, Γ plane is shown.

Through this model, failure is rapid while healing can be a much slower process. This follows if R is relatively small when Γ is small and F is less than a healing value F_h. This type of effect gives geological materials the memory they have of zones of earlier faulting. Here, $R(\Gamma, F)$ is taken in the form

$$(3.12)\quad R(\Gamma, F) = k(\Gamma, F)\left(-F + d_3(\frac{1}{2} - \Gamma) + \frac{d_2}{\Gamma} + \frac{d_1}{1-\Gamma} + d_4\right)\Gamma(1-\Gamma)$$

where $d_1, d_2, d_3 \text{and} d_4$ are material constants. The function k is chosen such that when Γ is small and $F < F_h$, k is small, insuring that healing is slow. Finally, $F_h$can be determined in terms of $d_1, d_2, d_3 \text{and} d_4$. Conceptually, these parameters depend on mineralogy, grain size, shape and packing.

We now show that the feedback associated with the coupling of shear stress (via incremental stress rheology) and rock competency naturally supports autonomous oscillation. Consider a simple shear system with the total rate of strain given by the sum of poroelastic and nonlinear viscous

contributions. The following ordinary differential equation for the shear stress follows from the incremental stress rheology of §3.1:

$$\frac{D\tau}{Dt} = \frac{G_f}{\mu(\Gamma)}(2\dot{\varepsilon}\mu(\Gamma) - \tau) \tag{3.13}$$

where τ, $\dot{\varepsilon}$, G_f and μ are the shear stress, total rate of shear strain, elastic shear modulus and shear viscosity, respectively. Shear viscosity is taken to be an increasing function of rock competency $\mu = \mu^*\Gamma^m$. The exponent m is taken as 8 to capture the large change in the order of magnitude of shear viscosity between intact and failed rock. The rate of shear strain is either taken to be a specified function of time or determined by the energy dissipation condition

$$\tau\dot{\varepsilon} = \dot{E} \tag{3.14}$$

where $\dot{E}$ is the rate of energy input.

Equations (3.8) and (3.13) form a strongly coupled set of nonlinear ordinary differential equations for the shear stress and rock competency that were integrated numerically by the fourth order Runga-Kutta technique with adaptive time stepping. Setting the RHS (3.13) to zero yields for constant $\dot{E}$ and the Druker-Prager failure function (B.2)

$$\Gamma = \left(\frac{(F+c)^2}{2\mu^*\dot{E}}\right)^{1/m} . \tag{3.15}$$

Fig. 16 illustrates the null curves for different values of $\dot{E}$. For small $\dot{E}$ the stress null curve (3.15) intersects the S-shape null curve $R = 0$ on the upper stable branch near $\Gamma = 1$ (competent rock), i.e., the competent rock viscosity μ^* is sufficiently low that the rate of energy input is equal to the rate of viscous energy dissipation (ductile flow). For very large $\dot{E}$, rock fails but the null curves intersect at the lower stable branch, i.e., the rock remains failed because of the very low shear viscosity needed to dissipate the required energy (aseismic faults). For intermediate values of $\dot{E}$, the null curves intersect at the unstable branch of $R = 0$. In this case, for a constant $\dot{E}$, rock fails and heals cyclicly (seismic faults). It is also possible that the null curves intersect at three distinct points. In this case, depending on the initial conditions of shear stress and rock competency, rock will either never fail or never heal. If a point (F, Γ) is above the null curve given by Equation (3.15), the shear stress increases, otherwise it decreases. Similarly, if a point (F, Γ) is to the right of the null curve $R = 0$, the rock competency decreases. These four cases suggest a classification of fault dynamics - intact stable sliding, failed stable sliding, multiple state and oscillatory sliding.

In the previous discussion, it is assumed that the shear viscosity is a function of rock competency only. In fact, shear viscosity depends strongly

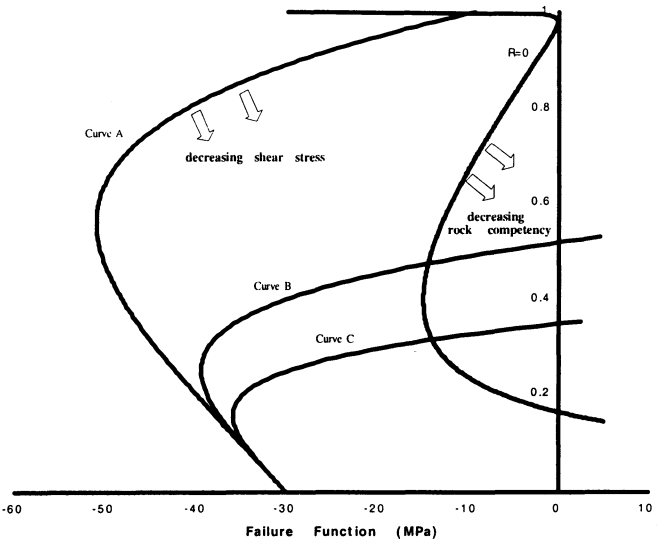

FIG. 16. *The null curves for equations (3.8) and (3.13) for different values of* $\dot{E}$.

on porosity and grain size distribution, i.e., $\mu^* = \mu^*(\Theta)$. Since grain size distribution, temperature dependent intrinsic viscosity of minerals and porosity change, the null curve given by Equation (3.15) can be viewed as an instantaneous function of rock texture. For example, as the grains get smaller due to gouge, the shear viscosity decreases and the stress null curve tends to intersect the S-shape curve ($R = 0$) at lower or higher Γ values depending on the S-shape curve. Similarly, particle size increase due to diagenesis can significantly change the behavior. Thus, gouge and diagenesis can determine which of the modes of fault behavior noted above are realized for a given fault system.

Failure is a fast process while healing is a slow one. Therefore, the coefficient k in Equation (3.12) is very large when the (F, Γ) point is to the right of the S-shape curve. On the other hand, for low shear viscosities (low Γ values) it is anticipated that the solution will follow Equation (3.15) rather than the S-shape curve ($R = 0$) because k is small in this region.

Equations (3.8) and (3.13) are generalized to include the fluid pressure, porosity and other components of the stress tensor (Tuncay, Khalil and Ortoleva 2001).

3.3. Fracture network statistical dynamics. We have developed a model of the probability for fracture length, aperture and orientation (Tuncay, Park, and Ortoleva 2000b). The model predicts the evolution of this probability in response to the changing stress, fluid pressure and rock properties as the basin changes. The fracture probability is used

to compute the permeability tensor. The latter affects the direction of petroleum migration, information key to finding new resources. It is central to planning infill drilling spacing and likely directions for field extension. It is key to the design of horizontal wells and the optimum rate of production in stress-sensitive reservoirs. Finally, the predicted distribution of fracture network statistics across a field is a necessary input to reservoir simulators used to optimize production.

The dynamics of the fracture network in our model is based on a statistical representation. For example, consider a set of fractures of length L with normal $\underline{n}$ for a 3-D spectrum of normal orientations. Then the rate of change for L in the rock-fixed frame takes the form

$$\frac{dL}{dt} = R(L, a, p, \Theta, \underline{\underline{\sigma}}) \tag{3.16}$$

where the fracture extension rate Rdepends on the normal stress σ, the wetting phase fluid pressure p and the texture Θ of the surrounding rock, and a is the aperture of the $\underline{n}$-fracture. A similar equation for the fracture aperture is developed (see Tuncay, Park and Ortoleva 2000b for further details).

Let η' be the number density of sites at which fractures may nucleate. By definition of the undeformed rock $\eta' = \eta$ (η being the original, depositional value of η') but η' can differ from η due to changes in rock texture from diagenesis or mechanical processes. In the simplest case where fracture nucleation sites are not created or destroyed, η' obeys the conservation equation $\partial\eta'/\partial t + \underline{\nabla} \cdot (\eta' \underline{u}) = 0$. In a macrovolume element of volume V there are $V\eta'$ fractures and hence a fracture void space $V\eta'\pi L^2 a$ where a and L are the aperture and length(radius) of the assumed penny-shaped fractures, respectively. To compute the dilatation, we focus on a fixed volume V_m of solids and follow its change in a time δt. The volume of the unfractured rock V_{unfr} is related to V_m and the porosity ϕ_m of the unfractured rock via $V_{unfr} = V_m + \phi_m V_{unfr}$. Hence, $V_{unfr} = V_m/(1 - \phi_m)$. The total volume V of the sample of rock containing V_m is then

$$V = (1 - \phi_m)^{-1} V_m + V\Delta \tag{3.17}$$

where $\Delta = \eta'\pi L^2 a$. With this, the volume of rock $V(t)$ at time t for fixed volume of solids V_m (considered incompressible and not to expand thermally or react) is given by

$$V(t) = V_m(1 - \phi_m)^{-1}(1 - \Delta). \tag{3.18}$$

Noting that

$$tr\underline{\underline{\dot{\varepsilon}}}^{(fr)} = \lim_{\delta t \to 0} \frac{V(t + \delta t) - V(t)}{V(t)\delta \mathrm{t}} \tag{3.19}$$

one obtains

$$tr\underline{\underline{\dot{\varepsilon}}}^{(fr)} = [1-\Delta]^{-1}\frac{D\Delta}{Dt} \tag{3.20}$$

where D/Dt is the material derivative, i.e., the derivative in the reference frame fixed to the solids.

The tensor character of the fracture mediated deformation is related to the directions of each fracture through its normal $\underline{n}$ to the fracture plane. Consider the expression

$$\dot{\varepsilon}_{kl}^{(fr)} = [1-\Delta]^{-1}\frac{D}{Dt}(\Delta n_k n_l). \tag{3.21}$$

Here D/Dt represents a material time derivative; however, now, it also must account for the rotation of the fracture normals as they change direction with flexure, shearing or other deformation. Note that the trace of this expression agrees with the earlier result for the dilatation. Finally, this expression agrees with simple cases wherein all fractures are parallel.

In our model, a finite (but representative) number of fracture orientations is accounted for. We use the fracture kinetics formulation of Ortoleva (1994a), and Sonnenthal and Ortoleva (1994). However, here we replace the least compressive stress in the formulation by the stress component normal to each fracture plane. This allows calculation of fracture length and aperture for each fracture orientation. For example, if we assume that only vertical fractures can occur as for a one dimensional problem, since the stress component normal to any vertical plane is the same because of the symmetry, an isotropic fracture network develops. In three dimensional problems, our proposed algorithm has the power to predict a complex fracture network with preferential orientations dictated by the structure of the stress tensor.

Since the fracture network is well defined, the anisotropic fracture permeability can be calculated approximately. The anisotropic fracture permeability of a fracture network consisting of a single fracture orientation is given by

$$K_{ij}^{fr} = \lambda(\delta_{ij} - n_i n_j) \tag{3.22}$$

where $\underline{n}$ is the unit normal to the fracture plane and $\underline{\underline{K}}^{fr}$ is the fracture permeability. The parameter λ can be approximated by

$$\lambda = \beta\phi_{fr}\frac{a^2}{12}. \tag{3.23}$$

Here β is a factor accounting for the connectivity of fractures. For large fracture lengths and dense networks β approaches unity whereas for small fracture lengths and low fracture densities it vanishes (Oda 1986). Oda (1985, 1986) proposed that this coefficient should be a function of a

dimensionless second order tensor of fracture geometry. He called this tensor the fabric tensor (Oda 1982). A discussion of this factor can be found in the papers of Oda (1985, 1986). In this study β is taken as unity. We assume that the total fracture permeability is obtained by summation of fracture permeabilities for all orientations and statistical classes multiplied by the fracture porosity which has been proposed previously by Chen et al. (1999). It is assumed that fluid flow is slow and the disturbance at fracture intersections is negligible. Summation is inadequate when the fracture density is lower than the percolation threshold (Berkowitz 1995; Odling 1992; Bour and Davy 1998). Another limitation is due to the surface roughness of fractures. In this study fracture aperture is assumed to be constant in a particular fracture. The spatial distribution of fracture aperture alters the fracture permeability. Waite et al. (1998) measured water flow through a sinusoidal fracture to compare sinusoidal flow with parallel plate flow. Their experimental and numerical results showed that a sinusoidal fracture has a significantly lower permeability and for the sinusoidal geometry the effective aperture is very close to the minimum value of the normal aperture. Thomson and Brown (1991) showed that the directional nonuniformities in the fracture surface are more important than the degree of surface roughness. Therefore Equation (3.23) should be viewed as a simple fracture permeability tensor to approximate dense fracture networks with relatively smooth fracture surface. Note that the fracture permeability tensor is obtained by post processing the fracture network characteristics.

We refer to Tuncay, Park and Ortoleva (2000b) for further details.

4. Conclusions. The examples presented above illustrate the complex set of factors that yield the disposition of the present-day fracture system. The latter is the product of a history of these factors and thereby often has little correlation with one or a few other present-day factors. The extensive set of rock and fluid parameters at each point within the crust makes inversion of seismic data difficult except for the simplest cases if our goal is to detect and characterize fractures remotely. It appears that the best hope of realizing remote fracture detection is to combine seismic data with 3-D RTM basin modeling. We believe that our Basin RTM simulator is uniquely suited for this purpose.

Acknowledgments. This project was supported by the Office of Science of the U.S .Department of Energy (grant # DE-FG02-91ER14175) and the Gas Research Institute (contract # 5097-260-3779).

REFERENCES

BERKOWITZ, B., 1995. Analysis of fracture network connectivity using percolation theory. *Mathematical Geology* 27:467–483.

BERRYMAN, J.G., 1980. Long-wavelength propagation in composite elastic media I. Spherical inclusions, *J. Acoust. Soc. Am.* 68: 1809–1819.

BERRYMAN, J.G., 1986. Effective medium approximation for elastic constants of porous solids with microscopic heterogeneity, *J. Appl. Phys.* 59: 1136–1140.

BOUR, O. AND P. DAVY, 1998. On the connectivity of three-dimensional fault networks. *Water Resource Research* 34: 2611–2622.

CHEN, M.M. BAI AND J.-C. ROEGIERS, 1999. Permeability tensors of anisotropic fracture networks. *Mathematical Geology* 31: 355–373.

DESAI, C.S. AND H.J. SIRIWARDANE, 1984. Constitutive laws for engineering materials. Prentice-Hall, Inc., Englewoods Cliffs, New Jersey.

DEWERS, T. AND P. ORTOLEVA, 1994a. Formation of stylolites, marl/limestone alternations, and dissolution (clay) seams by unstable chemical compaction of argillaceous carbonates. In *Diagenesis, IV,* Developments in Sedimentology 51, edited by K.H. Wolf and G.V. Chilingarian, 155–216. New York: Elsevier.

DEWERS, T. AND P. ORTOLEVA, 1994b. Nonlinear dynamical aspects of deep basin hydrology: Fluid compartment formation and episodic fluid release. American Journal of Science 294: 713–755.

DIETERICH, J.H., 1979. Modeling of rock friction 1. experimental results and constitutive equations. *Journal of Geophysical Research* 84: 2161–2168.

FREDRICH, J.T. AND B. EVANS, 1992. Strength recovery along simulated faults by solution transfer processes. In *33rd U.S. Rock Mechanics Symposium,* edited by J.R. Tillerson and W.R. Warersik, Balkema, Rotterdam, 121–130.

LARSON, K.W., D.W. WAPLES, H. FU, AND K. KODAMA, 1993. Predicting tectonic fractures and fluid flow through fractures in basin modeling. In *Basin Modeling: Advances and Applications,* edited by A. G. Dore, NPF Special Publications 3, 373–383. Elsevier, Amsterdam: Norwegian Petroleum Society.

LOGAN, J.M. AND L.W. TEUFEL, The effect of normal stress on the real area of contact during frictional sliding of rocks. *Pure and Applied Geophysics* 124: 471–486.

LUO, X. AND G. VASSEUR, 1996. Geopressuring mechanism of organic matter cracking: numerical modeling. *AAPG Bulletin* 80: 856–873.

LUO, X., G. VASSEUR, A. POUYA, V. LAMOUREUX-VAR, AND A. POLIAKOV, 1998. Elastoplastic deformation of porous medium applied to the modeling of compaction at basin scale. *Marine and Petroleum Geology* 15: 145–162.

MAUBEUGE, F. AND I. LERCHE, 1993. A north Indonesian basin: geo, thermal and hydrocarbon generation histories. *Marine and Petroleum Geology* 10: 231–245.

MAUBEUGE, F. AND I. LERCHE, 1994. Geopressure evolution and hydrocarbon generation in a north Indonesian basin: two-dimensional quantitative modeling. *Marine and Petroleum Geology* 104: 104–115.

ODA, M., 1982. Fabric tensor for discontinous geological materials. *Soils and Foundations* 22: 96–108.

ODA, M., 1985. Permeability tensor for discontinous rock masses. Geotechnique 35: 483–495.

ODA, M., 1986. An equivalent continuum model for coupled stress and fluid flow analysis in jointed rock masses. *Water Resources Research* 22: 1845–1856.

ODLING, N.E., 1992. Network properties of a two-dimensional natural fracture pattern. Pure and Applied Geophysics 138: 95–114.

ORTOLEVA, P., ED., 1990. Self-organization in geological systems. Earth-Science Reviews 29(1–4).

ORTOLEVA, P., 1992. *Nonlinear chemical waves.* New York: John Wiley and Sons.

ORTOLEVA, P., 1994a. *Geochemical self-organization.* New York: Oxford University Press.

ORTOLEVA, P., ED., 1994b. *Basin compartments and seals.* AAPG Memoir no. 61. Tulsa, Oklahoma: AAPG.

ORTOLEVA, P., 1998. *Basin compartment fundamentals,* Topical Report (Project No. GRI-97/0097). Chicago: Gas Research Institute.

OZKAN, G. AND P. ORTOLEVA, 2000. Evolution of gouge grain size distribution: A markov model. *Pure and Applied Geophysics* 157: 10510–10525.

OZKAN, G., K. TUNCAY, AND P. ORTOLEVA, 1998. Process-based fault seal/conduit prediction. In *1998 AAPG Annual Convention Abstracts* (CD-ROM format), Salt Lake City, UT, May 17–28, 1998.

PAYNE, D.F., K. TUNCAY, A. PARK, J. COMER, AND P. ORTOLEVA, 2000. A reaction-transport-mechanical approach to modelling the interrelationships between gas generation, overpressuring, and fracturing - Implications for the Upper Cretaceous natural gas reservoirs of the Piceance Basin, Colorado. *AAPG Bulletin* 84: 545–565.

RENARD, F. AND P. ORTOLEVA, 2001. Memory and the Self-Organizing Planet. In preparation.

RICE, J.R., 1975. Continuum mechanics and thermodynamics of plasticity in relation to microscale deformation mechanisms. *Constitutive equations in plasticity*, edited by A. S. Argon, 23–79. Cambridge, MA: MIT Press.

RICE, J.R. AND J.C. GU, 1983. Earthquake aftereffects and triggered seismic phenomena. *Pure and Applied Geophysics* 121: 187–219.

RICE, J.R. AND A. RUINA, 1983. Stability of steady frictional slipping. *Journal of Applied Mechanics* 50: 343–349.

ROBERTS, S.J. AND J.A. NUNN, 1995. Episodic fluid expulsion from geopressured sediments. *Marine and Petroleum Geology* 12: 195–204.

RUINA, A., 1983. Slip instability and state variable friction laws. *Journal of Geophysical Research* 88: 10359–10370.

SCHNEIDER, F., J.L. POTDEVIN, S. WOLF, AND I. FAILLE, 1996. Mechanical and chemical compaction model for sedimentary basin simulators. *Tectonophysics* 263: 307–317.

SONNENTHAL, E. AND P. ORTOLEVA, 1994. Numerical simulations of overpressured compartments in sedimentary basins. In *Basin compartments and seals*, AAPG Memoir no. 61, edited by P. Ortoleva, 403–416. Tulsa, Oklahoma: AAPG.

THOMSON, M.E. AND S.R. BROWN, 1991. The effect of anisotropic surface roughness on flow and transport in fractures. *Journal of Geophysical Research* 96: 21923–21932.

TSE, S.T. AND J.R. RICE, 1986. Crustal earthquake instability in relation to the depth variation of frictional slip properties. *Journal of Geophysical Research* 91: 9452–9472.

TUNCAY, K., A. PARK, AND P. ORTOLEVA, 2000a. Sedimentary basin deformation: An incremental stress approach. *Tectonophysics* 323: 77–104.

TUNCAY, K., A. PARK, AND P. ORTOLEVA, 2000b. A forward fracture model to predict fracture orientation and properties. *Journal of Geophysical Research* 105: 16719–16735.

TUNCAY, K. AND P. ORTOLEVA, 2000. Salt tectonics as a self-organizing process: A three dimensional reaction, transport and mechanics model. *Journal of Geophysical Research* 106: 803–818.

TUNCAY, K., A. KHALIL, AND P. ORTOLEVA, 2000. Failure, memory and cyclic fault movement. *Bulletin of Seismological Society of America* 91: 538–552.

UNGERER, P., J. BURRUS, B. DOLIGEZ, P.Y. CHENET, AND F. BESSIS, 1990. Basin evaluation by integrated two-dimensional modeling of heat transfer, fluid flow, hydrocarbon generation, and migration. *AAPG Bulletin* 74: 309–335.

WAITE, M.E., S. GE., H. SPETZLER, AND D.B. BAHR, 1998. The effect of surface geometry on fracture permeability: A case study using a sinusoidal fracture. *Geophysical Research Letters* 25: 813–816.

WANG, C. AND X. XIE, 1998. Hydrofracturing and episodic fluid flow in shale-rich basins - A numerical study. *AAPG Bulletin* 82: 1857–1869.

ZIENKIEWICZ, O.C. AND I.C. CORMEAU, 1974. Visco-plasticity and creep in elastic solids—A unified numerical solution approach. *International Journal for Numerical Methods for Engineering*, 8: 821–845.